



# Diamond surface conductivity: Properties, devices, and sensors

Christopher I. Pakes, Jose A. Garrido, and Hiroshi Kawarada

Hydrogen termination of diamond lowers its ionization energy, driving electron transfer from the valence band into an adsorbed water layer or to a strong molecular acceptor. This gives rise to *p*-type surface conductivity with holes confined to a subsurface layer of a few nanometers thickness. The transfer doping mechanism, the electronic behavior of the resulting hole accumulation layer, and the development of robust field-effect transistor (FET) devices using this platform are reviewed. An alternative method of modulating the hole carrier density has been developed based upon an electrolyte-gate architecture. The operation of the resulting “solution-gated” FET architecture in two contemporary applications will be described: the charge state control of nitrogen-vacancy centers in diamond and biosensing. Despite 25 years of work in this area, our knowledge of surface conductivity of diamond continues to develop.

## Introduction

Diamond, with a bandgap of 5.47 eV, is an insulating material when undoped. However, when terminated with hydrogen, the C–H bond at the terminated surface creates a dipole layer that induces a negative electron affinity reported to be as low as –1.3 eV and a concurrent lowering of the ionization energy to 4.2 eV.<sup>1</sup> While this phenomenon has led to significant interest in electron emission devices due to the ease with which electrons excited into the conduction band can be emitted from the surface, it additionally drives the transfer of electrons from the diamond valence band into the accepting state of an appropriate adsorbate layer on the diamond surface.<sup>2</sup> This gives rise to *p*-type surface conductivity carried by a resulting subsurface hole accumulation layer that extends a few nanometers into diamond and supports a carrier density of up to  $4 \times 10^{13} \text{ cm}^{-2}$ .<sup>2</sup> In addition to lowering the ionization energy sufficiently to facilitate electron transfer from the valence band into the adsorbate layer, the hydrogen termination passivates the surface by removing interfering surface states from the gap that would otherwise accept the transferred charge preventing them from contributing to free carriers in the diamond.

In its simplest form, the accumulation of holes and band bending at the surface of hydrogen-terminated diamond occurs as a consequence of charge transfer into an adsorbed water layer arising from exposure to air (**Figure 1a**).<sup>3</sup> It was shown in this case that surface charge transfer arises from an

electrochemical redox reaction between the adsorbed water layer and the diamond surface, a mechanism that is unique to hydrogenated diamond among semiconductor materials under standard atmospheric conditions.<sup>3</sup> Strobel et al. showed that *p*-type surface doping could also be achieved with fullerene ( $\text{C}_{60}$ ) and fluorinated fullerenes;<sup>4,5</sup> in this case, charge is transferred from the diamond valence band into the lowest unoccupied molecular orbital (LUMO) of the fullerene surface acceptor. While providing supporting evidence for the surface transfer doping model proposed as being responsible for the charge accumulation at the surface of diamond, this work additionally presented the possibility of using other molecular species as surface acceptors on the hydrogen-terminated diamond surface. Surface transfer doping of diamond with other molecular species, such as 7,7,8,8-tetracyanoquinodimethane and its fluorinated derivative,<sup>6</sup> and molecular heterolayers<sup>7</sup> have subsequently been demonstrated. Recently, Russell et al. have extended this work further to include the use of the transition metal oxide  $\text{MoO}_3$  as a surface electron acceptor material, which may offer improved stability and performance in diamond electronic devices.<sup>8</sup>

## Interfacial energy level alignment

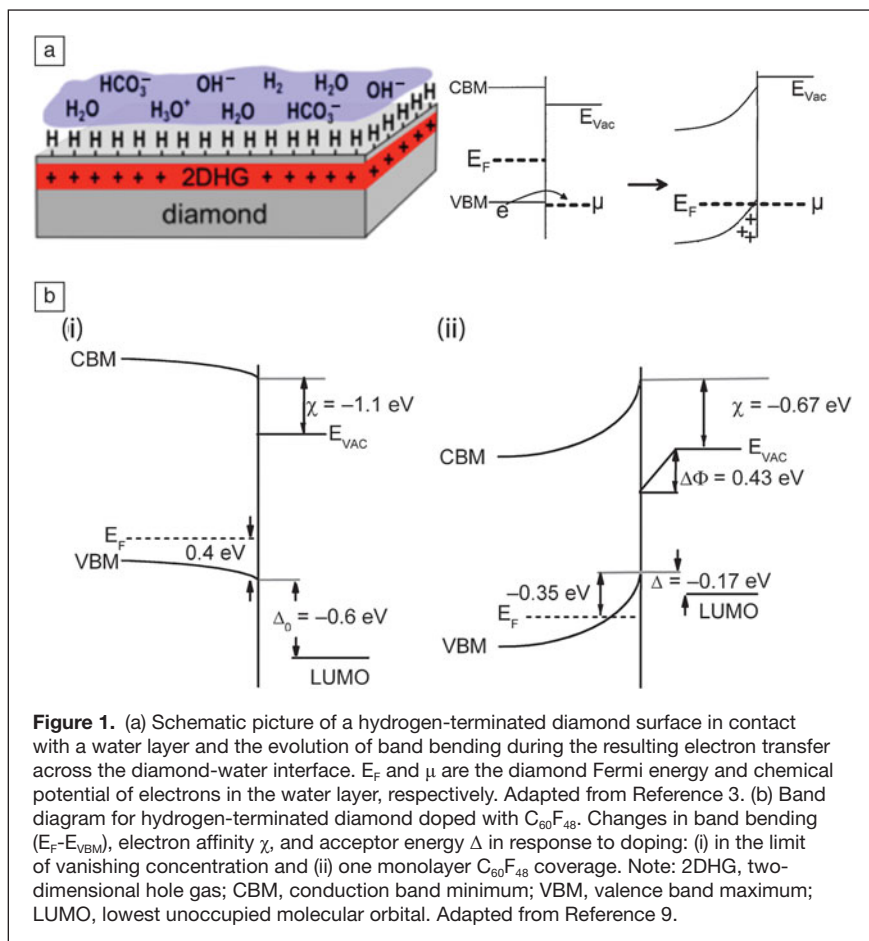
In contrast to doping with an adsorbed water layer, organic molecules provide a simpler acceptor system that can be probed using standard surface analysis techniques to aid the

Christopher I. Pakes, Department of Physics, La Trobe University, Victoria, Australia; c.pakes@latrobe.edu.au

Jose A. Garrido, Walter Schottky Institute and Physics Department, Technische Universität München, Germany; garrido@wsi.tum.de

Hiroshi Kawarada, Department of Electronics and Photonics Systems and Department of Nanoscience and Nanotechnology, Waseda University, Japan; kawarada@waseda.jp

DOI: 10.1557/mrs.2014.95



understanding of the surface charge transfer mechanism. This has been achieved by Edmonds et al. using the fluorofullerene  $C_{60}F_{48}$  as a strong molecular acceptor.<sup>9</sup> The introduction of the strongly electronegative fluorine atoms to the cage of fullerene induces a large electron affinity in the fluorofullerenes.  $C_{60}F_{48}$  has an electron affinity of 4.06 eV in vapor form,<sup>10</sup> higher than any of the other fluorofullerenes, and making it a very effective surface acceptor at the hydrogen-terminated diamond surface. The resulting diamond hole concentration at saturation differs for the different fluorofullerenes and appears to scale with the electron affinity of the fluorofullerene.<sup>5</sup>

When doped with  $C_{60}F_{48}$ , the underlying hole concentration reaches a saturation value equivalent to that for air-induced surface conductivity for a fluorofullerene coverage of only about 0.4 monolayers. This allows the electronic energy level structure at the diamond-fluorofullerene interface to be probed using surface-sensitive photoemission techniques. By using synchrotron-based C1s core level photoelectron spectroscopy, Edmonds et al. observed two distinct molecular charge states of  $C_{60}F_{48}$ , one corresponding to ionized molecules that participate in surface charge transfer and the other to neutral molecules that do not.<sup>9</sup> The relative concentrations of these states gives a direct measure of the fluorofullerene doping efficiency, while their binding energy informs the shift in the

corresponding LUMO of the two charge states as a function of coverage. At the same time, measured shifts in the binding energy of the C1s core level associated with the underlying diamond surface informs the level of band bending as a result of charge accumulation during doping.

Using this information, and the fact that doping of the fluorofullerene is governed by Fermi-Dirac statistics, the energy level alignment at the diamond/fluorofullerene interface has been explained (Figure 1b).<sup>9</sup> The position of the LUMO of neutral  $C_{60}F_{48}$  was determined to lie initially 0.6 eV below the valence band maximum (VBM). Since the neutral LUMO is the relevant acceptor level for transfer doping, this energy represents a negative acceptor energy,  $\Delta_0 = -0.6$  eV, implying a high initial doping efficiency (equal to one) and suggesting that there should be no freeze-out of carriers at low temperature. This is an important result in the context of low-temperature transport. As the fluorofullerene coverage is increased, the doping efficiency drops to zero above a critical coverage, limiting the ultimately achievable hole carrier concentration. This is a consequence of an upward shift of the neutral LUMO with coverage due to the formation of a doping-induced surface dipole  $\Delta\Phi$  arising from the charge separation across the diamond/molecule

interface<sup>11</sup> in conjunction with band bending ( $E_F - E_{VBM}$ ). The two quantities that ultimately determine the achievable hole density are thus the initial acceptor energy and the areal capacitance associated with the interfacial charge separation. The initial acceptor energy for a specific acceptor layer is influenced by the value of the negative electron affinity of the underlying hydrogen-terminated surface; variation in the quality of the hydrogen termination may therefore be responsible for the range of saturation hole sheet densities that have been reported by different groups in the literature.

### Transport properties

There have been a number of studies of the transport properties of surface conducting diamond, focusing primarily on the measurement of temperature dependence of the hole sheet density and carrier mobility.<sup>12,13</sup> Temperature-dependent transport measurements have generally resulted in an exponential decrease in the conductivity as the temperature is reduced, suggesting conduction occurs via hopping between localized states as a result of high levels of surface disorder.<sup>12,13</sup> As a result, the low temperature behavior of this system has not been extensively probed. Recently, Yamaguchi et al.<sup>14</sup> showed that an evolution from semiconducting to metallic conduction can be obtained as the hole sheet density is increased using

an electrolyte gated architecture, discussed in detail later. Yamaguchi's work has demonstrated experimentally that a high hole carrier concentration can be maintained at low temperature, consistent with the fact that the negative initial acceptor energy prevents carrier freeze out. With the availability of high-quality samples, this motivates future studies of the low-temperature properties of the hole accumulation layer. Hole mobility measurements have consistently resulted in mobilities of up to  $300 \text{ cm}^2 \text{V}^{-1} \text{s}^{-1}$ .<sup>15</sup> The low levels of mobility result from ionized impurity scattering due to the nearby charged surface acceptors,<sup>16</sup> a major drawback of this system; an alternative doping scheme analogous to modulation doping as employed in GaAs-based semiconductor heterostructures could resolve this issue, but is yet to be realized.

While it is well known that the hole accumulation is confined to the near-surface region of diamond, a significant number of papers in the field refer to the hole accumulation layer as being two-dimensional despite there being no clear experimental evidence that this is the case. Density functional theory calculations have predicted the formation of a two-dimensional hole band at the surface of hydrogen-terminated (100) diamond;<sup>17</sup> however, the lack of low temperature transport measurements means this is yet to be unambiguously confirmed. A number of alternative measurements have been made to elucidate the presence of quantized energy eigenstates in the hole layer based upon field-emission<sup>18</sup> and scanning tunneling spectroscopy<sup>19</sup> techniques, supported by theoretical estimates of the eigenvalues via self-consistent solution of the Poisson-Schrödinger equation for the hole accumulation layer.<sup>20,21</sup> However, the dimensionality of the surface-conducting layer remains an issue of contemporary interest.

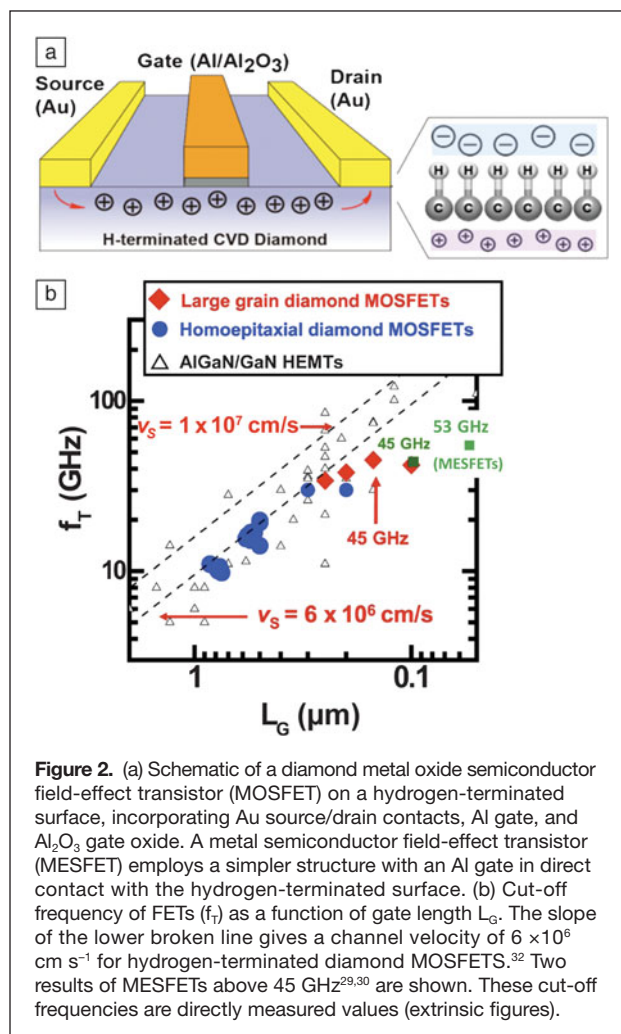
### Field-effect transistor devices on the hydrogen-terminated diamond surface

Following the first report of surface conductivity in diamond,<sup>2</sup> the work of many research groups focused on the removal of surface conductivity in order to maintain a highly resistive substrate. It was not until four years after the report of surface conductivity that the first robust field-effect transistor (FET) operation with pinch-off characteristics (i.e., with a sufficiently high bias at the gate, the channel no longer contains free carriers, and the current drops to zero) was reported in a metal-semiconductor (MES) FET.<sup>22,23</sup> In this architecture, a hole current between two Au ohmic contacts was controlled using an Al-based Schottky gate in direct contact with the hydrogen-terminated surface. The MESFET showed logic operation,<sup>24</sup> and a relatively high breakdown voltage of near 200 V was also demonstrated.<sup>25</sup> Since the prototype MESFET structure is very simple, if undoped diamond and a process for hydrogen termination had been available in the late 1940s, diamond may well have been the first transistor material.

The electronic behavior of metallic contacts on the hydrogen-terminated diamond surface is governed by the height of the resulting Schottky barrier. The dependence of the Schottky barrier height on the electrode material clearly demonstrates

a Schottky limit where the metal work function (or electronegativity) governs the barrier height.<sup>24,26</sup> This indicates a very low density of surface states ( $<10^{11} \text{ cm}^{-2}$ ), which is a necessary condition for operation of metal-insulator-semiconductor (MIS) or metal oxide semiconductor (MOS) FET device architectures, shown schematically in **Figure 2a**. Metals with high work function such as Au (5.1 eV) show low Schottky barrier heights, typically less than 0.2 eV<sup>24,26</sup> and are advantageous for the formation of ohmic contacts. In contrast, metals with low work function such as Al (4.3 eV) exhibit a Schottky barrier of nearly 1 eV. By using gate metals with different Schottky barrier heights, enhancement mode to depletion mode FETs have been fabricated on the same surface, and enhancement/depletion-type invertors and other logic circuits can be obtained.<sup>24</sup>

High-frequency FET operation was realized in an Al gate MESFET,<sup>27</sup> representing the first operation of a FET at GHz frequencies in a pure carbon semiconductor. Subsequent improvements in cut-off frequency,  $f_T$ , have been achieved via a reduction in gate length while maintaining the same basic device structure (Figure 2b). Through this route, cut-off





frequencies in the range 20–53 GHz have been achieved in MESFET,<sup>28–30</sup> MISFET, and MOSFET<sup>31,32</sup> architectures. From the slope of  $f_T$  as a function of gate length, a hole velocity of  $5 \times 10^6 \text{ cm s}^{-1}$  can be estimated equal to one half of the maximum carrier velocity of diamond. Despite a substantial shift in effort toward the development of graphene-based FETs, the directly measured cut-off frequencies of hydrogen-terminated diamond devices remain comparable to those currently achieved in graphene, illustrating the achievements in the design and fabrication of CVD diamond FETs. Additionally, source-drain current densities exceeding  $1 \text{ A mm}^{-1}$  have been achieved in hydrogen-terminated diamond MOSFETs,<sup>33,34</sup> a level equivalent to contemporary semiconductor devices based on Si, GaAs, InGaAs, GaN, and graphene. Naturally, the current densities in diamond devices are highly dependent on the achievable hole sheet density which, in general, is higher for (111)- and (110)-oriented surfaces compared to the (100) surface; this arises because the areal density of the dipole moment arising from the C–H bond is 20–30% higher for the former surfaces.<sup>33</sup> As a result, higher current densities are typically reported for devices fabricated on (111)- and (110)-oriented diamond.

Despite its seeming fragility, air-induced surface conductivity in hydrogen-terminated diamond has been used to develop a number of applications through the device architectures that we have described. The C–H bond and also surface adsorbates are stable in air and remain so at the metal/diamond and insulator/diamond interfaces. Hole accumulation may be maintained after growth of a gate dielectric via atomic layer deposition (ALD).<sup>35</sup> For example, MOSFETs with an  $\text{Al}_2\text{O}_3$  gate dielectric formed by ALD at a temperature of  $450^\circ\text{C}$ , far above the desorption temperature of the adsorbates, have been demonstrated and can operate at temperatures up to  $450^\circ\text{C}$ .<sup>36</sup> Through the development of these processes, the surface conductivity can be utilized for high-power, high-temperature applications.

### Solution-gate devices on the hydrogen-terminated diamond surface

#### Electrolyte gating of the surface conductivity

As an alternative to gating with a solid-state contact, the surface conductivity of hydrogen-terminated diamond can be modulated using an electrolyte-gate,<sup>37</sup> and this approach has recently led to several important applications. Here, the hydrogen-terminated surface is immersed in an aqueous electrolyte along with a gate electrode, and control of the surface conductivity is achieved by using the gate to modulate the diamond/electrolyte interfacial

potential.<sup>38</sup> This mechanism is illustrated schematically in **Figure 3a**.

The Fermi energy  $E_F$  in the diamond surface is fixed by a potentiostat, relative to an Ag/AgCl reference electrode. Therefore, usually no thermodynamic equilibrium exists between  $E_F$  and the redox couple responsible for the surface conductivity in air. For an increasing negative potential,  $U_G$ , applied to the gate electrode, the position of  $E_F$  at the diamond surface is driven further into the diamond valence band, increasing the accumulation of holes at the diamond/electrolyte interface. If the applied potential is reversed and a more positive gate potential is applied,  $E_F$  at the diamond surface will be pushed eventually above the valence band maximum, and the hole accumulation diminishes.

Thus, in contrast to the situation in air,<sup>3</sup> charge transfer across the interface has no influence on the formation of the surface conductivity in an electrolyte under potential control.<sup>38</sup> Instead, we have described a situation in which the hole accumulation layer is induced by capacitive polarization of the interface. Electrochemical impedance spectroscopy measurements at the hydrogenated-diamond/electrolyte interface have confirmed that the interface behaves like an ideal capacitor<sup>39,40</sup> for which the hole carrier density is approximately proportional to the applied gate potential. Hall effect measurements have additionally confirmed the linear relationship between the carrier density and the applied gate voltage at negative  $U_G$ .<sup>40</sup>

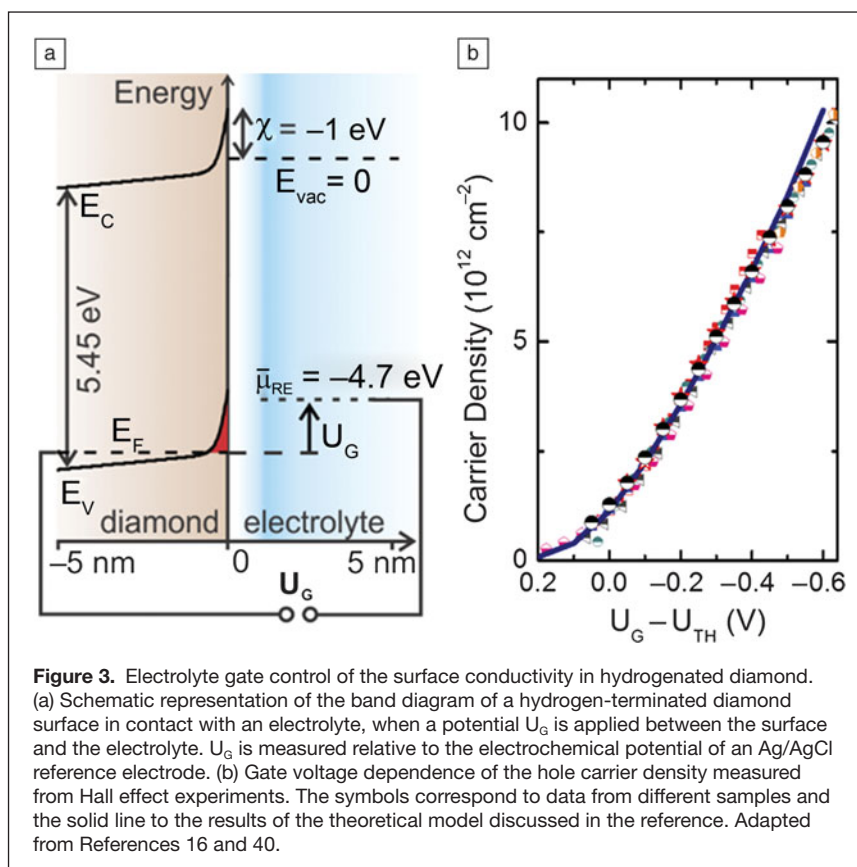


**Figure 3.** Electrolyte gate control of the surface conductivity in hydrogenated diamond. (a) Schematic representation of the band diagram of a hydrogen-terminated diamond surface in contact with an electrolyte, when a potential  $U_G$  is applied between the surface and the electrolyte.  $U_G$  is measured relative to the electrochemical potential of an Ag/AgCl reference electrode. (b) Gate voltage dependence of the hole carrier density measured from Hall effect experiments. The symbols correspond to data from different samples and the solid line to the results of the theoretical model discussed in the reference. Adapted from References 16 and 40.

shown in Figure 3b, with an interfacial capacitance of about  $2 \mu\text{F cm}^{-2}$  deduced from the slope of this linear dependence, in good agreement with impedance spectroscopy measurements.<sup>39,40</sup> Due to this relatively high interfacial capacitance, hole carrier densities as high as  $10^{13} \text{ cm}^{-2}$  can be obtained, motivating the development of solution-gated field-effect transistor (SGFET) devices.<sup>40</sup>

### Electrostatic control of the charge state of NV centers in diamond SGFETs

The nitrogen-vacancy (NV) center in diamond has drawn considerable interest during recent years in diverse fields such as quantum information processing, single-spin magnetometry, and plasmonics.<sup>41–43</sup> Most of these applications exploit the fact that the spin state of the negatively charged NV center ( $\text{NV}^-$ ) can be initialized and read out optically. However, this state has been observed to become unstable, turning into the neutral charge state  $\text{NV}^0$  under various kinds of laser illumination, close to the surface, or at high implantation densities. In order to engineer large-scale quantum processors using this architecture, it is therefore an outstanding goal to reliably be able to control the charge state of an NV center.

Motivated by the ability to control of the surface conductivity of hydrogenated diamond that can be achieved using an aqueous electrolyte gate,<sup>40</sup> it is possible to design a dynamic method to manipulate the charge state of single NV centers with such an electrolytic gate electrode.<sup>44</sup> Similar to the case of a diamond SGFET, in this case, a potential can be applied between a nitrogen-implanted and subsequently H-terminated diamond immersed in an electrolyte and a reference electrode in the electrolyte, as illustrated in Figure 4a. The shift in Fermi energy of the diamond induced by the applied voltage changes the extent of band bending at the diamond surface. Thus, the position of the Fermi level with respect to the charge transition level of the NV centers is modified by the applied gate voltage.<sup>44</sup> The charge transition levels  $\text{NV}^{+/0}$  and  $\text{NV}^{0/-}$  correspond to the energies at which a NV center changes its charge state from

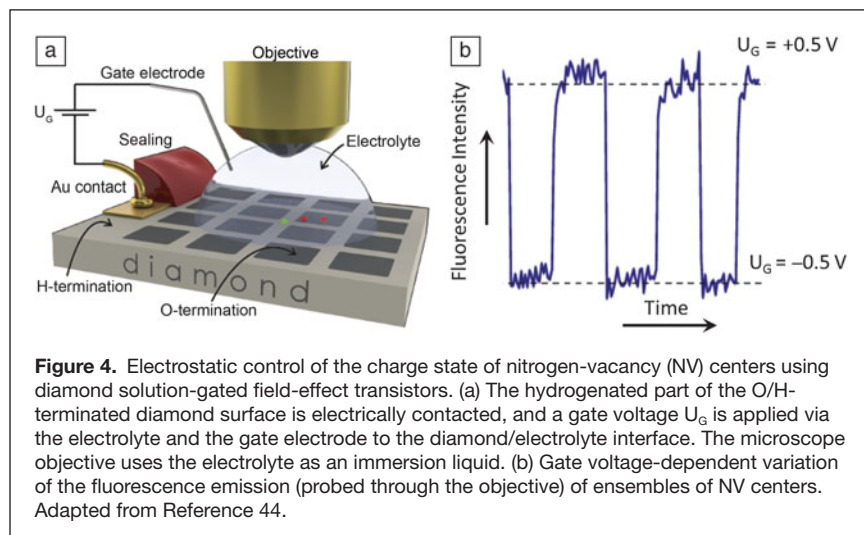
positive to neutral and from neutral to negative, respectively.<sup>45</sup> By using the external gate voltage, it is possible to shift  $E_F$  across the charge transition levels in a way that a NV center at a certain distance from the diamond surface goes from the positive charge state through the neutral state and to the negative charge state.<sup>44</sup>

Figure 4b shows a time series of the  $\text{NV}^-$  fluorescence obtained in a region of high implantation dose while the electrolyte gate voltage is repeatedly switched between 0.5 V and  $-0.5$  V. The observed reversible fluorescence change has been discussed in terms of the discharge of the negatively charged centers into  $\text{NV}^0$  and the subsequent reversed charging from  $\text{NV}^0$  to  $\text{NV}^-$ .<sup>44</sup> Thus, electrolyte-gating of surface conductive diamond offers very versatile and reversible control of the charge state of embedded NV centers in diamond, providing an important toolkit for the use of NV centers in diamond-based spintronics or sensing applications.<sup>41</sup>

### Biosensing and bioelectronics applications of diamond SGFETs

Arrays of diamond SGFETs (Figure 5a), based upon the electrolyte gating concept described previously, have shown great potential for biosensors and bioelectronic applications.<sup>16</sup> Sensing applications have the potential to profit enormously from employing FETs as transducing devices, mainly due to their intrinsic amplification capability, illustrated by the transistor curves shown in Figure 5b, and the high integration offered by semiconductor technology. Due to its maturity as a commercial semiconductor material, most of the work with SGFETs has been done using Si technology. However, there are several disadvantages of using Si technology for this application, such as a low electrochemical stability and relatively high electronic noise, motivating the search for more suitable materials. Diamond appears to be an ideal candidate for the development of highly sensitive SGFETs.

Unlike other semiconductors and metals, the hydrogen-terminated diamond surface shows remarkable chemical and electrochemical stability. This makes the need for a protective dielectric layer unnecessary and therefore, as we have noted previously, interfacial capacitances formed at the electrolyte/diamond interface can be high, leading to devices with enhanced transconductance and thus gate sensitivity.<sup>16,40,46</sup> In addition to the transconductance, the low-frequency noise performance of an SGFET determines the device sensitivity (i.e., the minimum signal at the gate that can be detected). It has been shown that similar to other semiconductors and metals, the noise spectral density of diamond SGFETs exhibits a  $1/f$  dependence.<sup>16,47</sup> Considering the typical bandwidth used in biosensors and bioelectronic applications (1 Hz to 5 kHz), the minimum gate noise obtained for diamond SGFETs shows an RMS value of



15  $\mu\text{V}$ ,<sup>47</sup> which is similar to that measured with low-noise Si devices. Further, diamond surfaces can be effectively modified with organic and bio-organic molecules,<sup>48</sup> enabling the preparation of diamond SGFETs with a variety of surface functional groups, thus paving the way for the development of SGFET-based sensors that are selective to certain analytes.

Using this potential for sensing of surface conductive diamond films, a broad range of diamond SGFETs biosensors have been demonstrated. The pH and ion sensitivity of diamond SGFETs have been extensively studied and discussed in terms of a pH dependent surface charge.<sup>37,49–51</sup> Taking advantage of the pH sensitivity of diamond surfaces, SGFET-based sensors modified with enzymes have been shown to be capable of detecting biologically relevant analytes such as penicillinase or the neurotransmitter acetylcholine.<sup>52</sup> Further, diamond SGFETs modified with DNA and RNA monolayers have been used for DNA and protein detection.<sup>53,54</sup> Several types of diamond surface termination were applied, resulting in the immobilization of short DNA/RNA within a few nm from the surface. Owing to the high interfacial capacitance, the change in the surface charge caused by the hybridization of DNA/RNA and protein binding to DNA/RNA aptamers can be efficiently detected,<sup>54</sup> confirming that the solid-surface channel of the SGFET is an ideal device for DNA and protein sensing.

More recently, diamond SGFETs have been used to study the electrical activity of different electrogenic cells,<sup>16,55</sup> such as cardiac muscle (cardiomyocyte) cells cultured on diamond transistor arrays. Three days after cell seeding, the cells formed a densely packed layer covering the active areas of the transistors. The devices below this cell carpet were still fully functional, and the simultaneous recording of the drain-source currents of all transistors at a common operation point showed

almost concurrent and repeated spikes on all working transistors (Figure 5c), corresponding to the action potentials of the cells, which are known to be spontaneously generated and propagate across the confluent cell culture. This work demonstrated that diamond offers various advantages as a new material for biohybrid devices for the detection of cell signals, which may find use in important medical applications such as neuroprostheses as well as for fundamental research on communication processes in neuronal networks.

## Conclusions and future outlook

Since its demonstration, surface conductivity in diamond has presented researchers in the field with both challenges in understanding its origin and opportunities for its application. Despite the fact that research in this area has been ongoing for 25 years, knowledge of this system continues to develop as do applications of contemporary interest. The performance of diamond surface electronic devices in many ways remains on par with that of materials such as graphene, and we can expect this trend to continue in the future. Improvements in the quality of the hydrogen-terminated surfaces, so that metallic conduction is maintained down to low temperatures, presents an opportunity to examine whether the conductivity is due to the predicted delocalized two-dimensional hole band at the diamond surface and, if so, to explore the magneto-transport properties of this system.

Furthermore, calculations suggest that for the highest hole sheet densities that have been reported, the corresponding volume carrier density is about  $2 \times 10^{20} \text{ cm}^{-3}$ , which is close to the critical carrier density for the superconductivity in boron-doped diamond. A combination of careful surface preparation and optimization of the hole sheet density from knowledge of the underlying doping mechanism will drive the investigation of whether surface-conducting diamond can exhibit superconductivity.

Finally, unlike conventional semiconductor electronics, where the choice of donor or acceptor is restricted to atomic species that can be incorporated into the crystal lattice of the semiconductor, surface transfer doping of diamond offers the possibility of exploiting a potentially wide choice of synthetic molecular systems as acceptors with properties that can be systematically modified to introduce functional properties in addition to being dopants. The use of organic acceptors in diamond devices is in its infancy, but there is considerable scope to engineer a new generation of functional devices on this platform.

## References

1. J.B. Cui, J. Ristein, L. Ley, *Phys. Rev. Lett.* **81**, 429 (1998).
2. M.I. Landstrass, K.V. Ravi, *Appl. Phys. Lett.* **55**, 975 (1989).
3. F. Maier, M. Riedel, B. Mantel, J. Ristein, L. Ley, *Phys. Rev. Lett.* **85**, 3472 (2000).
4. P. Strobel, M. Riedel, J. Ristein, L. Ley, *Nature* **430**, 439 (2004).

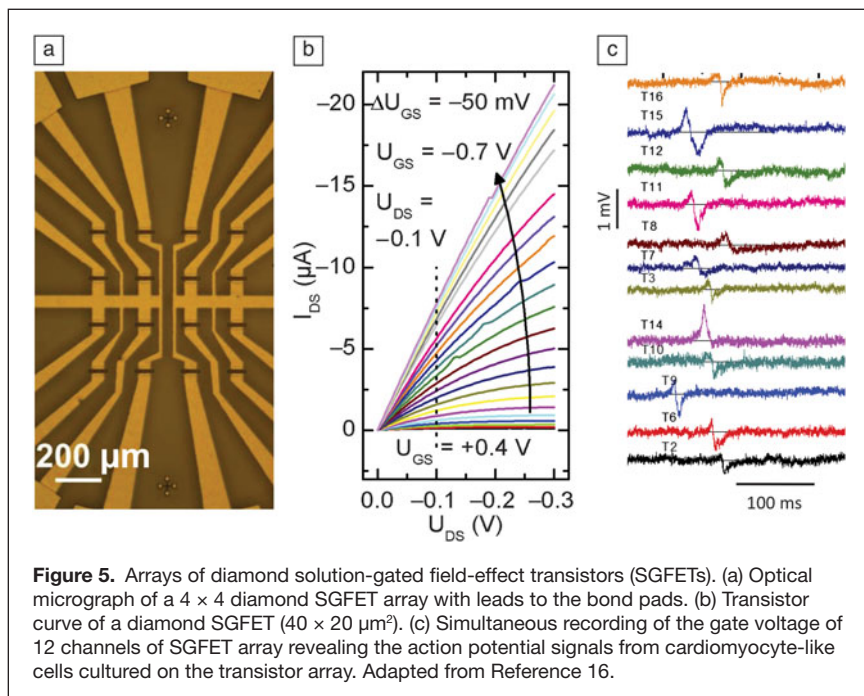


**Figure 5.** Arrays of diamond solution-gated field-effect transistors (SGFETs). (a) Optical micrograph of a  $4 \times 4$  diamond SGFET array with leads to the bond pads. (b) Transistor curve of a diamond SGFET ( $40 \times 20 \mu\text{m}^2$ ). (c) Simultaneous recording of the gate voltage of 12 channels of SGFET array revealing the action potential signals from cardiomyocyte-like cells cultured on the transistor array. Adapted from Reference 16.



5. P. Strobel, M. Riedel, J. Ristein, L. Ley, O. Boltalina, *Diam. Relat. Mater.* **14**, 451 (2005).
6. W. Chen, D. Qi, X. Gao, A.T.S. Wee, *Prog. Surf. Sci.* **84**, 279 (2009).
7. D. Langley, Y. Smets, C.B. Stark, M.T. Edmonds, A. Tadich, K.J. Rietwyk, A. Schenk, M. Wanke, Q.-H. Wu, P. Barnard, L. Ley, C.I. Pakes, *Appl. Phys. Lett.* **100**, 032103 (2012).
8. S.A.O. Russell, L. Cao, D. Qi, A. Tallaie, K.G. Crawford, A.T.S. Wee, D.A. Moran, *Appl. Phys. Lett.* **103**, 202112 (2013).
9. M.T. Edmonds, M. Wanke, A. Tadich, H.M. Vulling, K.J. Rietwyk, P.L. Sharp, C.B. Stark, Y. Smets, A. Schenk, Q.-H. Wu, L. Ley, C.I. Pakes, *J. Chem. Phys.* **136**, 124701 (2012).
10. R. Mitsumoto, K. Seki, T. Araki, E. Ito, Y. Ouchi, Y. Achiba, K. Kikuchi, S. Yajima, S. Kawasaki, F. Okino, H. Touhara, H. Kurosaki, T. Sonoda, H. Kobayashi, *J. Electron. Spectrosc. Relat. Phenom.* **78**, 453 (1996).
11. M.T. Edmonds, C.I. Pakes, S. Mammadov, W. Zhang, A. Tadich, J. Ristein, L. Ley, *Appl. Phys. Lett.* **98**, 102101 (2011).
12. C.E. Nebel, C. Sauerer, F. Ertl, M. Stutzmann, C.F.O. Graeff, P. Bergonzo, O.A. Williams, R. Jackman, *Appl. Phys. Lett.* **79**, 4541 (2001).
13. J.A. Garrido, T. Heimbeck, M. Stutzmann, *Phys. Rev. B* **71**, 245310 (2005).
14. T. Yamaguchi, E. Watanabe, H. Osato, D. Tsuya, K. Deguchi, T. Watanabe, H. Takeya, Y. Takano, S. Kurihara, H. Kawarada, *J. Phys. Soc. Jpn.* **82**, 074718 (2013).
15. B. Rezek, H. Watanabe, C.E. Nebel, *Appl. Phys. Lett.* **88**, 042110 (2006).
16. M. Dankerl, M.V. Hauf, M. Stutzmann, J.A. Garrido, *Phys. Status Solidi A* **209**, 1631 (2012).
17. D. Alfonso, D.A. Drabold, S.E. Ulloa, *Phys. Rev. B* **51**, 14669 (1995).
18. L. Gan, E. Baskin, C. Saguy, R. Kalish, *Phys. Rev. Lett.* **96**, 196808 (2006).
19. A. Bolker, C. Saguy, M. Tordjman, L. Gan, R. Kalish, *Phys. Rev. B* **83**, 155434 (2011).
20. C.E. Nebel, B. Rezek, A. Zrenner, *Phys. Status Solidi A* **201**, 2432 (2004).
21. M.T. Edmonds, C.I. Pakes, L. Ley, *Phys. Rev. B* **81**, 085314 (2010).
22. H. Kawarada, M. Aoki, I. Itoh, *Appl. Phys. Lett.* **65**, 1563 (1994).
23. H. Itoh, H. Kawarada, *Jpn. J. Appl. Phys.* **34**, 4677 (1995).
24. H. Kawarada, *Surf. Sci. Rep.* **26**, 205 (1996).
25. P. Gluche, A. Aleksov, A. Vescan, W. Ebert, E. Kohn, *IEEE Electron Device Lett.* **18**, 547 (1997).
26. K. Tsugawa, H. Noda, K. Hirose, H. Kawarada, *Phys. Rev. B* **81**, 045303 (2010).
27. H. Taniuchi, H. Umezawa, T. Arima, M. Tachiki, H. Kawarada, *IEEE Electron Device Lett.* **22**, 390 (2001).
28. A. Aleksov, A. Denisenko, U. Spitzberg, T. Jenkins, W. Ebert, E. Kohn, *Diam. Relat. Mater.* **11**, 382 (2002).
29. K. Ueda, M. Kasu, Y. Yamauchi, T. Makimoto, M. Schwitters, D.J. Twitchen, G.A. Scarsbrook, S.E. Coe, *IEEE Electron Device Lett.* **27**, 570 (2006).
30. S.A.O. Russell, S. Sharabi, A. Tallaie, D.A.J. Moran, *IEEE Electron Device Lett.* **33**, 570 (2012).
31. H. Matsudaira, S. Miyamoto, H. Ishizaka, H. Umezawa, H. Kawarada, *IEEE Electron Device Lett.* **25**, 480 (2004).
32. K. Hiram, H. Takayanagi, S. Yamauchi, Y. Jingu, H. Umezawa, H. Kawarada, *IEEE IEDM* (2007), p. 873.
33. H. Kawarada, *Jpn. J. Appl. Phys.* **51**, 090111 (2012).
34. K. Hiram, M. Kasu, *Jpn. J. Appl. Phys.* **51**, 090112 (2012).
35. D. Kueck, A. Schmidt, A. Denisenko, E. Kohn, *Diam. Relat. Mater.* **19**, 166 (2010).
36. A. Hiraiwa, A. Daicho, S. Kurihara, Y. Yokoyama, H. Kawarada, *J. Appl. Phys.* **112**, 124504 (2012).
37. H. Kawarada, Y. Araki, T. Sakai, T. Ogawa, H. Umezawa, *Phys. Status Solidi A* **185**, 79 (2001).
38. J.A. Garrido, A. Hartl, M. Dankerl, A. Reitingner, M. Eickhoff, A. Helwig, G. Muller, M. Stutzmann, *J. Am. Chem. Soc.* **130**, 4177 (2008).
39. J.A. Garrido, S. Nowy, A. Hartl, M. Stutzmann, *Langmuir* **24**, 3897 (2008).
40. M. Dankerl, A. Lippert, S. Birner, E.U. Stuetzel, M. Stutzmann, J.A. Garrido, *Phys. Rev. Lett.* **106**, 196103 (2011).
41. G. Balasubramanian, P. Neumann, D. Twitchen, M. Markham, R. Kolesov, N. Mizuochi, J. Isoya, J. Achard, J. Beck, J. Tessler, V. Jacques, P.R. Hemmer, F. Jelezko, J. Wrachtrup, *Nat. Mater.* **8**, 383 (2009).
42. V. Acosta, P. Hemmer, *MRS Bull.* **38** (2) (2013).
43. J.R. Maze, P.L. Stanwix, J.S. Hodges, S. Hong, J.M. Taylor, P. Cappellaro, L. Jiang, M.V. Gurudev Dutt, E. Togan, A.S. Zibrov, A. Yacoby, R.L. Walsworth, M.D. Lukin, *Nature* **455**, 644 (2008).
44. B. Grotz, M.V. Hauf, M. Dankerl, B. Naydenov, S. Pezzagna, J. Meijer, F. Jelezko, J. Wrachtrup, M. Stutzmann, F. Reinhard, J.A. Garrido, *Nat. Commun.* **3**, 729 (2012).
45. M.V. Hauf, B. Grotz, B. Naydenov, M. Dankerl, S. Pezzagna, J. Meijer, F. Jelezko, J. Wrachtrup, M. Stutzmann, F. Reinhard, J.A. Garrido, *Phys. Rev. B* **83**, 081304 (2011).
46. K.-S. Song, G.-J. Zhang, Y. Nakamura, K. Furukawa, T. Hiraki, J.-H. Yang, T. Funatsu, I. Ohdomari, H. Kawarada, *Phys. Rev. E* **74**, 041919 (2006).
47. M.V. Hauf, L.H. Hess, J. Howgate, M. Dankerl, M. Stutzmann, J.A. Garrido, *Appl. Phys. Lett.* **97**, 093504 (2010).
48. J.A. Garrido, in *CVD Diamond for Electronic Devices and Sensors*, R.S. Sussmann, Ed. (Wiley, Chichester UK, 2009).
49. J.A. Garrido, A. Hardt, S. Kuch, M. Stutzmann, O. Williams, R. Jackmann, *Appl. Phys. Lett.* **86**, 073504 (2005).
50. M. Dankerl, A. Reitingner, M. Stutzmann, J.A. Garrido, *Phys. Status Solidi RRL* **2**, 31 (2008).
51. A. Hartl, J.A. Garrido, S. Nowy, R. Zimmermann, C. Werner, D. Horinek, R. Netz, M. Stutzmann, *J. Am. Chem. Soc.* **129**, 1287 (2007).
52. A. Hartl, B. Baur, M. Stutzmann, J.A. Garrido, *Langmuir* **24**, 9898 (2008).
53. S. Kuga, J.H. Yang, H. Takahashi, K. Hiram, T. Iwasaki, H. Kawarada, *J. Am. Chem. Soc.* **130**, 13251 (2008).
54. H. Kawarada, A.R. Ruslinda, *Phys. Status Solidi A* **208**, 2005 (2011).
55. M. Dankerl, S. Eick, B. Hofmann, M. Hauf, S. Ingebrandt, A. Offenhäusser, M. Stutzmann, J.A. Garrido, *Adv. Funct. Mater.* **19**, 2915 (2009). □

MRS OnDemand®

## NEW CONTENT AVAILABLE

## The 2014 MRS Spring Meeting OnDemand

MRS OnDemand now includes a large sampling of the rich materials science content from the 2014 MRS Spring Meeting. Watch presentations from the Meeting **FREE**, for a limited time, complete with audio and presentation materials.

- ▶ Select MRS Award Talks
- ▶ Technology Innovation Forum VII
- ▶ Fred Kavli Distinguished Lectureship in Nanoscience
- ▶ Women in Materials Science & Engineering Breakfast
- ▶ Select Symposium X Talks
- ▶ 7 Tutorial Sessions
- ▶ Select Talks from 25 Technical Sessions



Plus, view interviews, news and highlights from the 2014 MRS Spring Meeting via MRS TV.

[www.mrs.org/ondemand](http://www.mrs.org/ondemand)